



# Precise Molecular Design of a Pair of New Regioisomerized Fluorophores With Opposite Fluorescent Properties

Zexin Wang<sup>1,2†</sup>, Renfu Li<sup>3†</sup>, Li Chen<sup>1†</sup>, Xin Zhai<sup>2</sup>, Wei Liu<sup>1,4</sup>, Xiang Lin<sup>1,5</sup>, Liwei Chen<sup>1</sup>, Nannan Chen<sup>1</sup>, Shitao Sun<sup>2</sup>, Zhenli Li<sup>2</sup>, Jinle Hao<sup>2</sup>, Xueyuan Chen<sup>3\*</sup>, Bin Lin<sup>2\*</sup> and Lijun Xie<sup>1\*</sup>

<sup>1</sup>Fujian Provincial Key Laboratory of Screening for Novel Microbial Products, Fujian Institute of Microbiology, Fuzhou, China, <sup>2</sup>Department of Medicinal Chemistry, School of Pharmaceutical Engineering, Shenyang Pharmaceutical University, Shenyang, China, <sup>3</sup>CAS Key Laboratory of Design and Assembly of Functional Nanostructures, and Fujian Key Laboratory of Nanomaterials, Fujian Institute of Research on the Structure of Matter, Chinese Academy of Sciences, Fuzhou, China, <sup>4</sup>School of Pharmacy, Fujian Medical University, Fuzhou, China, <sup>5</sup>Hengyang Medical School, Institute of Cytology and Genetics, University of South China, Hengyang, China

## OPEN ACCESS

### Edited by:

Lucas Rodrigues,  
University of São Paulo, Brazil

### Reviewed by:

Xinhua Cao,  
Xinyang Normal University, China  
Apurba Lal Koner,  
Indian Institute of Science Education  
and Research, Bhopal, India

### \*Correspondence:

Xueyuan Chen  
xchen@fjirsm.ac.cn  
Bin Lin  
randybinlin@gmail.com  
Lijun Xie  
lijunxie8224@outlook.com

<sup>†</sup>These authors have contributed  
equally to this work and share first  
authorship

### Specialty section:

This article was submitted to  
Physical Chemistry and Chemical  
Physics,  
a section of the journal  
Frontiers in Chemistry

Received: 27 November 2021

Accepted: 30 December 2021

Published: 20 January 2022

### Citation:

Wang Z, Li R, Chen L, Zhai X, Liu W,  
Lin X, Chen L, Chen N, Sun S, Li Z,  
Hao J, Chen X, Lin B and Xie L (2022)  
Precise Molecular Design of a Pair of  
New Regioisomerized Fluorophores  
With Opposite Fluorescent Properties.  
Front. Chem. 9:823519.  
doi: 10.3389/fchem.2021.823519

Aggregation-induced emission (AIE) has attracted much attention in the past 2 decades. To develop novel AIE-active materials, ACQ-to-AIE transformation via regioisomerization is one of the most straightforward method. However, most of the reported ACQ-to-AIE transformations are achieved by migrating bulky units. In this work, a facile conversion was realized by migrating a small pyrrolidinyl group from *para*- to *ortho*-position on the rofecoxib scaffold. As a result, a pair of new isomers named **MOX2** and **MOX4** exhibited AIE behavior and ACQ activity, respectively. Moreover, **MOX2** also showed solvatochromic, mechanochromic, and acidochromic properties with reversible multi-stimulus behavior. Single crystal X-ray analysis of **MOX2** revealed that the molecular conformation and its packing mode were responsible for the AIE emission behavior. Further investigation indicated that **MOX2** showed high lipid droplets staining selectivity. Taken together, the current work not only provides a new design philosophy for achieving ACQ-to-AIE conversion by migrating a small pyrrolidinyl group but also presents a promising candidate **MOX2** for potential applications such as in security ink, optical recording and biological applications.

**Keywords:** aggregation-induced emission, aggregation-caused quenching, regioisomerization, multi-stimuli responsive, LDs imaging

## INTRODUCTION

Aggregation Induced Emission (AIE) materials have been successfully developed in different research fields since it was discovered by Tang's group back in 2001 (Luo et al., 2001; Hong et al., 2009; Hong et al., 2011; Mei et al., 2015; Arathi et al., 2016; Mallick et al., 2017; Lou and Yang, 2020). To date, a variety of AIE luminogens (AIEgens) have been reported (Lim et al., 2016; Choi et al., 2020; Li J. et al., 2020) for their inherent characteristics of high brightness in solid states by suppressing extensive  $\pi$ - $\pi$  stackings in their packing mode (Yuan et al., 2014; Mei et al., 2015), which would otherwise result in aggregation-caused quenching (ACQ) of the fluorophores (Hong et al., 2009; Yuan et al., 2010). These AIEgens varied greatly in terms of their chemical structures, including tetraphenylethylene (TPE) (Feng H. T. et al., 2018; La et al., 2018; Wu et al., 2018), triphenylamine (TPA) (Zhang et al., 2013; Cao et al., 2014; Zhang Y. et al., 2014), cyano-substituted diarylethene

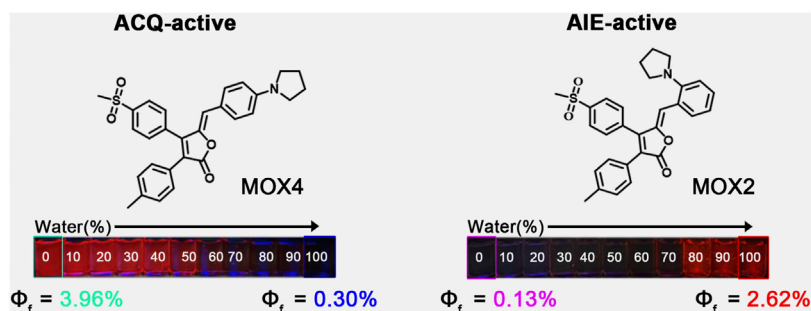


**FIGURE 1** | A pair of new regioisomerized fluorophores with opposite fluorescent properties.

(Shen et al., 2013; Zhang X. et al., 2014; Lu et al., 2015), 2,3,4,5-tetraphenylsiloles (Chen et al., 2014), silole (Chang et al., 2015), distyrylanthracene (Niu et al., 2015; Xiong et al., 2015), and anthracene derivatives (Lu et al., 2010; Zhang et al., 2011; Li A. et al., 2019), conjugated polymers (Ravindran and Somanathan, 2017; Wang et al., 2018), and so on. Modification of the existing AIE scaffolds is the most popular strategy for constructing new AIEgens (Mei et al., 2015). In addition to this strategy, transforming ACQ molecules into AIE-active materials also provides a direct way to design highly bright AIEgens due to the rich source of ACQ (Yuan et al., 2010; Zong et al., 2016; Liu et al., 2017; Lu et al., 2019; Li Y. et al., 2020; Pratihar et al., 2020; Wang et al., 2020; Huang et al., 2021; Long et al., 2021; Zhang et al., 2021).

Traditionally, ACQ-to-AIE transformation can be achieved by integrating bulky substituents into ACQ molecules to avoid strong  $\pi$ - $\pi$  stackings or by introducing twisted AIEgens (Dhokale et al., 2015; Gomez-Duran et al., 2015; Feng X. et al., 2018) and propeller-shaped molecules into ACQ fluorophores (Ma et al., 2016; Wang et al., 2020). However, integration of twisted AIEgens prolongs the  $\pi$  system thus it would probably change the already satisfactory fluorescent properties of the original ACQ molecules. Therefore, it will be highly desirable to achieve ACQ-to-AIE conversion without extending its conjugated system too much. Some progresses have been made along this line for the past decade (Sasaki et al., 2017; Li Y. et al., 2020). Among them, ACQ-to-AIE conversion was realized by Tang's group recently through a regioisomerization strategy via shifting a molecular rotor in the end position of a planar core of dithieno [2,3-a:3',2'-c] benzo [i] phenazine (TBP) to the bay position (Li Y. et al., 2020). The same strategy was utilized by Xu's group to achieve ACQ-to-AIE conversion through changing the substituted position of a benzanthrone moiety from the meta-position to the *ortho*-position on the perylenetetra-carboxylic diimide core (Long et al., 2021). Similarly, Prasad's group also realized ACQ-to-AIE transformation by changing a cyano group from the *para*-position to the meta-position on the same phenyl group (Pratihar et al., 2020). Despite the great examples above, the successful cases of the regioisomerization of small units are still rare (Pratihar et al., 2020). Therefore, it is still necessary to develop

more examples of ACQ-to-AIE conversion to guide the design of novel AIEgen materials.

Herein, we report our recent work on the realization of ACQ-to-AIE transformation by migrating a small pyrrolidine group from *para*- to *ortho*-position based on the rofecoxib scaffold. The resulting compounds **MOX4** with *para*-substitution showed ACQ effect while compound **MOX2** with *ortho*-substitution exhibited AIE activity (**Figure 1**). Moreover, **MOX2** also showed multi-stimulus fluorescent responsive properties, such as mechanochromic, acidochromic properties. In addition, its potential applications have been presented. This work is expected to provide a new guidance on designing AIE-type materials.

## EXPERIMENTAL

### Materials and Instrumentation

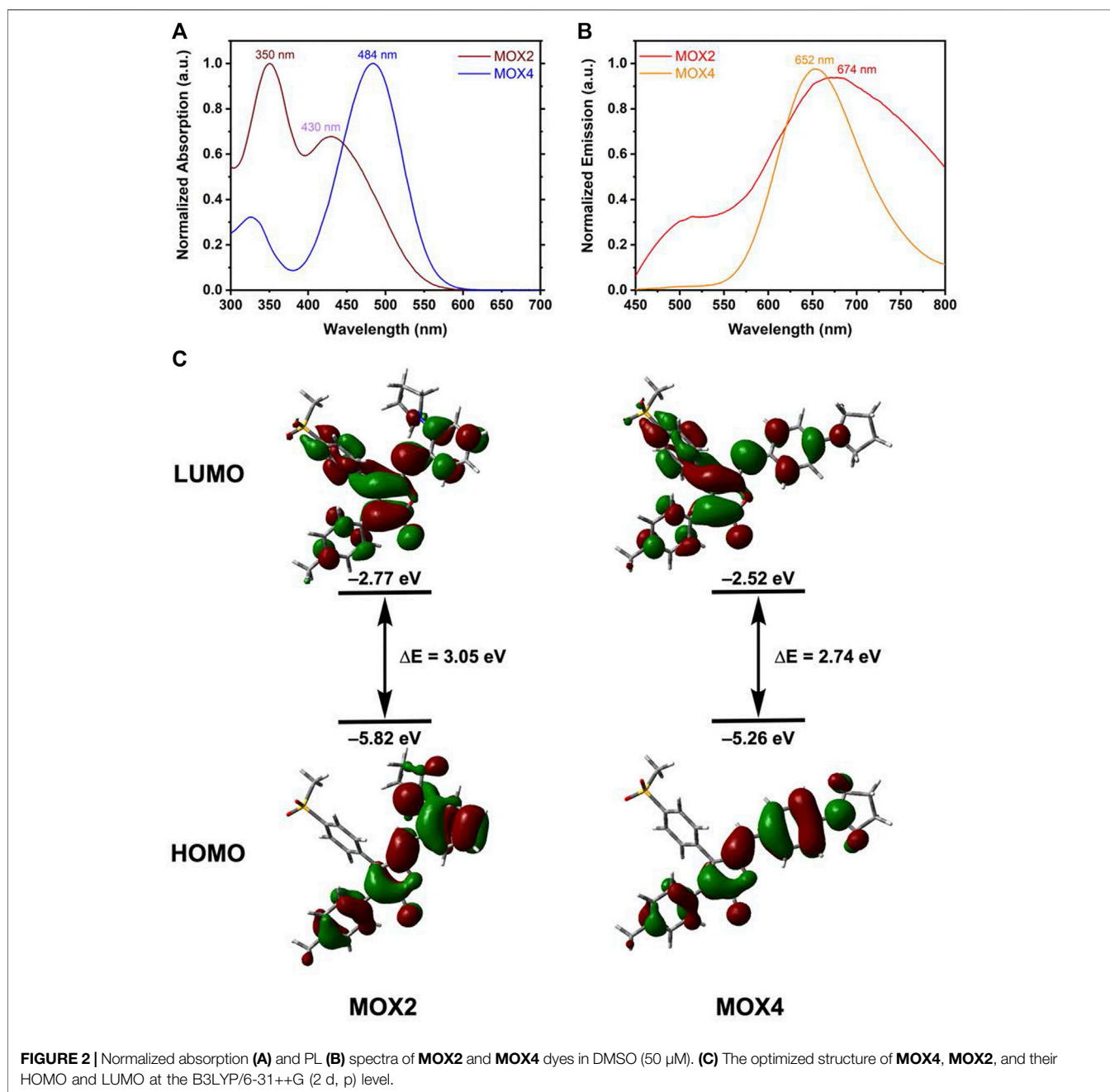
All commercial reagents and solvents were used as received. Compounds *p*-tolylacetic acid and 2-bromo-4'-methanesulfonyl acetophenone were purchased from Shanghai Macklin Biochemical Co., Ltd. and Shanghai Bidepharm Co., Ltd., respectively. Various benzaldehydes with different substituted groups were purchased from Shanghai Shaoyuan Co., Ltd. Reactions were magnetically stirred and monitored on a TLC Silica gel 60G F254 plate from Millipore Sigma (United States). All other reagents and solvents were purchased from Sigma-Aldrich (United States) and used without further purification, unless otherwise stated. Photoluminescence (PL) spectra were recorded on a Varioskan LUX 3020-80110. Differential scanning calorimetry (DSC) were obtained on a DSC STAR system at a heating rate of 15°C/min from 40°C to 500°C under a high purity nitrogen atmosphere. Powder X-ray diffraction (PXRD) patterns were recorded on a Rigaku (D/MaX-3B) diffractometer. Single-crystal X-ray diffraction was conducted with Bruker D8 Quesr/Venture diffraction with  $\lambda = 0.77\text{\AA}$  (MoK $\alpha$ ). Lipid droplets (LDs) imaging was performed with a Nikon Ti-E&C2 scanning unit.  $^1\text{H}$  NMR and  $^{13}\text{C}$  NMR spectra were measured on a Bruker AV 600 spectrometer in appropriated deuterated chloroform solution at room temperature with the solvent residual proton signal as a standard. High resolution mass spectra (HRMS) were recorded

on a GCT premier CAB048 mass spectrometer operating in MALDI-TOF mode.

## Synthesis and Characterization

The synthetic route of compounds is outlined in **Scheme 1**. The key intermediate **MOX** was synthesized in a one-step reaction involving cyclization of esters *via* 2-bromo-4'-methanesulfonylacetophenone and *p*-methyl phenylacetic acid in the presence of triethylamine and DBU. Finally, the target compounds **MOX2** and **MOX4** were prepared via Knoevenagel condensation reaction. (**General procedure**). Piperidine, 3 drops, was added to a mixture of 0.140 g (0.0004 mol) of intermediate

(**MOX**) and 0.140 g of 2-(1-Pyrrolidinyl) bezaldehyde in 10 ml of methanol, and the mixture was stirred at room temperature for 12 h in dark atmosphere. The mixture was then cooled, and the precipitate was filtered off and washed with methanol on a filter. The yellow powder (**MOX2**, 0.1001 g) was obtained with the yield 72%. The DSC thermogram of powder **MOX2** showed only one endothermic peak that corresponds to the melting point ( $T_m = 203.6^\circ\text{C}$ ) (**Supplementary Figure S12**).  $^1\text{H}$  NMR (600 MHz,  $\text{DMSO-}d_6$ )  $\delta$  8.09 (d,  $J = 8.3$  Hz, 2H), 7.89 (d,  $J = 8.8$  Hz, 1H), 7.72 (d,  $J = 8.3$  Hz, 2H), 7.26 (d,  $J = 23.8$  Hz, 3H), 7.17 (d,  $J = 8.1$  Hz, 2H), 7.05–6.89 (m, 2H), 6.04 (s, 4H), 3.06 (s, 3H), 2.28 (s, 1H), 1.76 (s, 4H).  $^{13}\text{C}$  NMR (151 MHz,  $\text{DMSO-}d_6$ )  $\delta$  168.3, 150.3, 148.8,



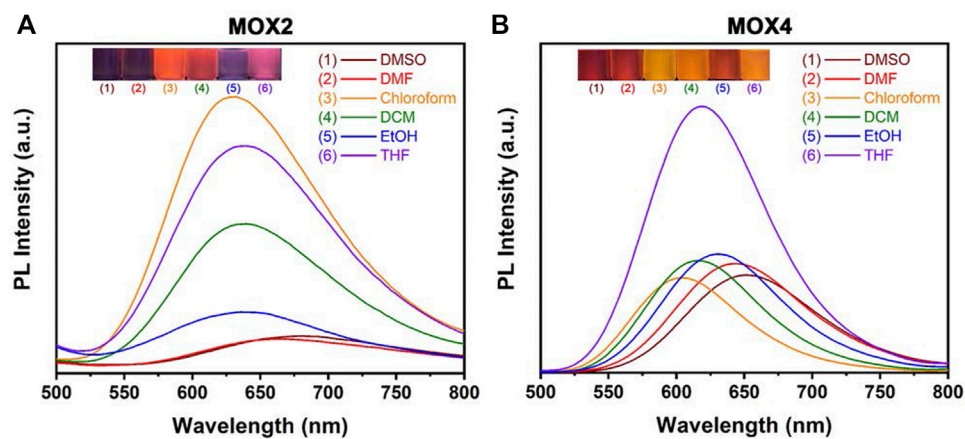


**FIGURE 3** | PL spectra of compounds **MOX2** (A) and **MOX4** (B) in various solvents (50  $\mu$ M), such as DMSO, DMF, chloroform, DCM, EtOH, THF, respectively. Inset: photograph of **MOX2** (A) and **MOX4** (B) in various solvents with UV irradiation ( $\lambda = 365$  nm).

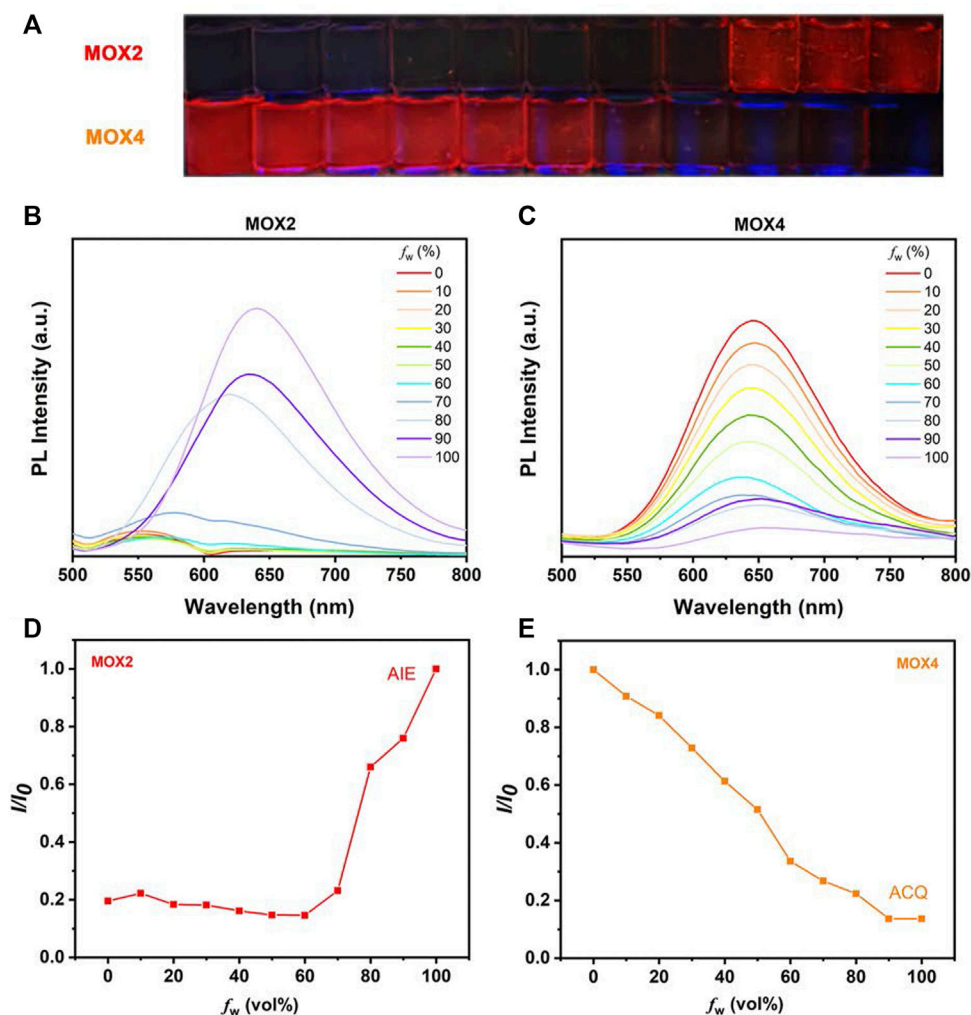


**FIGURE 4** | (A) The photos in different solvent states of **MOX2** and **MOX4** at 365 nm (10  $\mu$ M). (B) The **MOX2** PL spectra as a function of the water fraction in DMSO. (C) The **MOX4** PL spectra as a function of the water fraction in DMSO. (D) Variation in PL intensity ( $I/I_0$ ) of **MOX2** with  $f_w$  (%), where  $I_0$  is the luminescence intensity in pure  $H_2O$ . (E) Variation in PL intensity ( $I/I_0$ ) of **MOX4** with  $f_w$  (%), where  $I_0$  is the luminescence intensity in pure DMSO.

**TABLE 1** | Photoluminescence QY of **MOX4** and **MOX2**.

Compounds	QY (%)
<b>MOX4</b> (0% water)	3.96
<b>MOX4</b> (100% water)	0.30
<b>MOX2</b> (0% water)	0.13
<b>MOX2</b> (100% water)	2.62

146.6, 142.1, 139.2, 136.1, 131.5, 130.6, 130.5, 129.5, 129.3, 128.0, 126.5, 124.8, 123.2, 120.6, 116.8, 111.9, 52.6, 43.7, 24.9, 21.4. HR-MS (ESI): calcd for  $C_{29}H_{27}NO_4S$ : 486.1734 [(M + H)<sup>+</sup>], found: 486.1813. The red powder (**MOX4**, 0.1230 g) was synthesized following the general procedure with the yield 88%. The DSC thermogram of powder **MOX4** showed only one endothermic peak that corresponds to the melting point ( $T_m = 231.3^\circ\text{C}$ ) (**Supplementary Figure S12**). <sup>1</sup>H NMR (600 MHz, DMSO-*d*<sub>6</sub>)  $\delta$  8.05 (d,  $J = 8.1$  Hz, 2H), 7.67 (dd,  $J = 8.2, 3.9$  Hz, 4H), 7.20 (d,  $J = 8.0$  Hz, 2H), 7.13 (d,  $J = 8.0$  Hz, 2H), 6.61 (d,  $J = 8.7$  Hz, 1H), 5.94 (s, 1H), 3.33 (s, 3H), 2.27 (s, 4H), 1.97 (s, 4H). <sup>13</sup>C NMR (151 MHz, DMSO-*d*<sub>6</sub>)  $\delta$  168.4, 148.7, 148.6, 144.2, 141.9, 138.5, 136.3, 133.0, 130.8, 129.5, 129.2, 128.0, 127.0, 122.4, 120.5, 115.2, 112.5, 47.7, 43.8, 25.4, 21.3. HR-MS (ESI): calcd for  $C_{29}H_{27}NO_4S$ : 486.1734 [(M + H)<sup>+</sup>], found: 486.1771. The final products were characterized by <sup>1</sup>H NMR, <sup>13</sup>C NMR, high-resolution mass spectrometry and single-crystal X-ray diffraction. The relevant data are collected from the original spectra and listed in the Support Information (**Supplementary Figures S1–S6**).

## RESULTS AND DISCUSSION

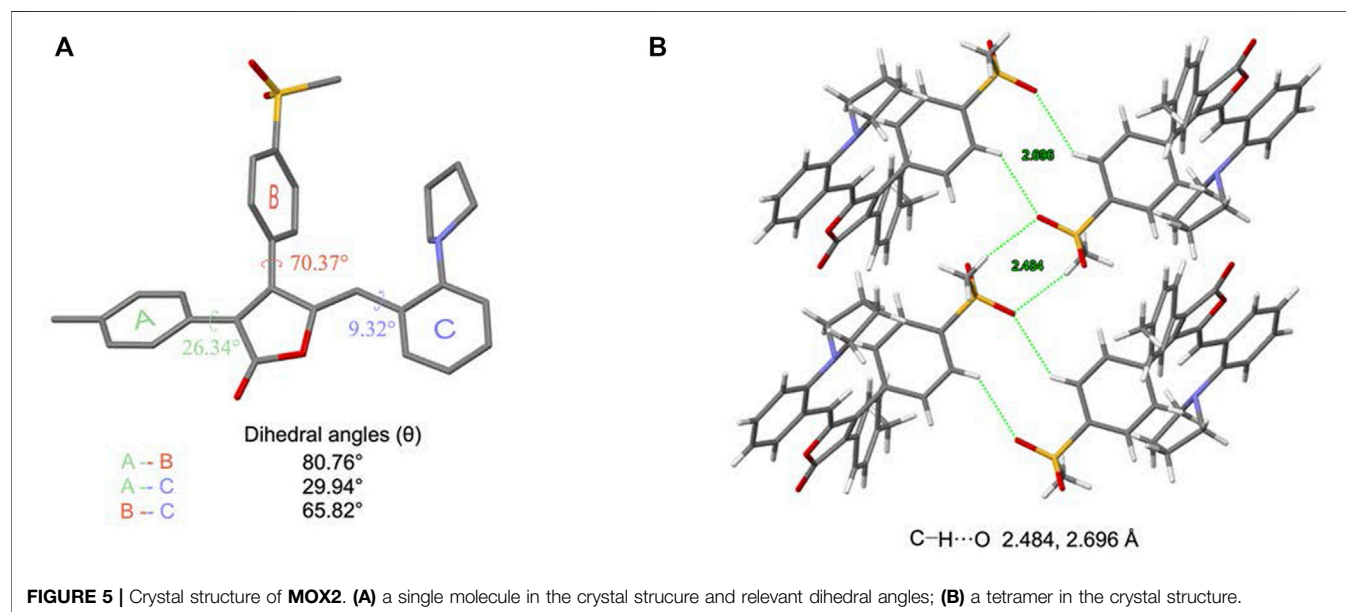
### Absorption and PL Intensity in Solution

As displayed in **Figure 2A**, **MOX2** had two absorption bands at 350 and 430 nm, respectively. The high energy band was

attributed to the  $\pi$ - $\pi$  transition while the low energy band was probably caused by the internal charge transfer (ICT) (Pati et al., 2013; Pati et al., 2015). In contrast, **MOX4** has only one maximum absorption band at 484 nm. In terms of emission, **MOX2** had a maximum PL intensity at 674 nm, slightly red-shifted compared to 652 nm of **MOX4** (**Figure 2B**). Another attractive feature of **MOX2** was its large Stokes shifts ( $13,675\text{ cm}^{-1}$ ) in dimethyl sulfoxide (DMSO) as displayed in **Supplementary Table S1**, which may be beneficial for overcoming the self-quenching of traditional fluorophores (Li P. et al., 2019). We carried out an experiment of 50  $\mu\text{M}$  concentration, this intensity was consistent with the Beer-Lambert's plot (**Supplementary Figure S7**). To provide insight into regioisomerization of the pyrrolidine group in compounds **MOX2** and **MOX4** on their photophysical properties, density functional theory (DFT) calculations at the B3LYP/6-311++G (2 d,p) level were carried out (Lee et al., 1988). The ICT was evident in comparison between the highest occupied molecular orbital (HOMO) and the lowest unoccupied molecular orbital (LUMO). The energy band gap was determined to be 3.05 and 2.75 eV for **MOX2** and **MOX4**, respectively, which was consistent with our experimental absorption data (**Figure 2C**).

### Solvatochromic Properties

The UV-vis absorption and PL spectra of **MOX2** and **MOX4** were measured in different solvents, such as DMSO, dimethylformamide (DMF), chloroform, dichloromethane (DCM), ethanol (EtOH), tetrahydrofuran (THF). The photophysical data were summarized in **Supplementary Table S1**. As the solvent varied from chloroform to DMSO, the  $\lambda_{abs}$  of **MOX2**, and **MOX4** displayed minor changes, indicating that their ground states are hardly affected by the solvent polarity (**Supplementary Figure S8**). In contrast, the PL spectra of **MOX2** and **MOX4** exhibited different maximum wavelengths in different solvents (**Figure 3**). With the solvent polarity



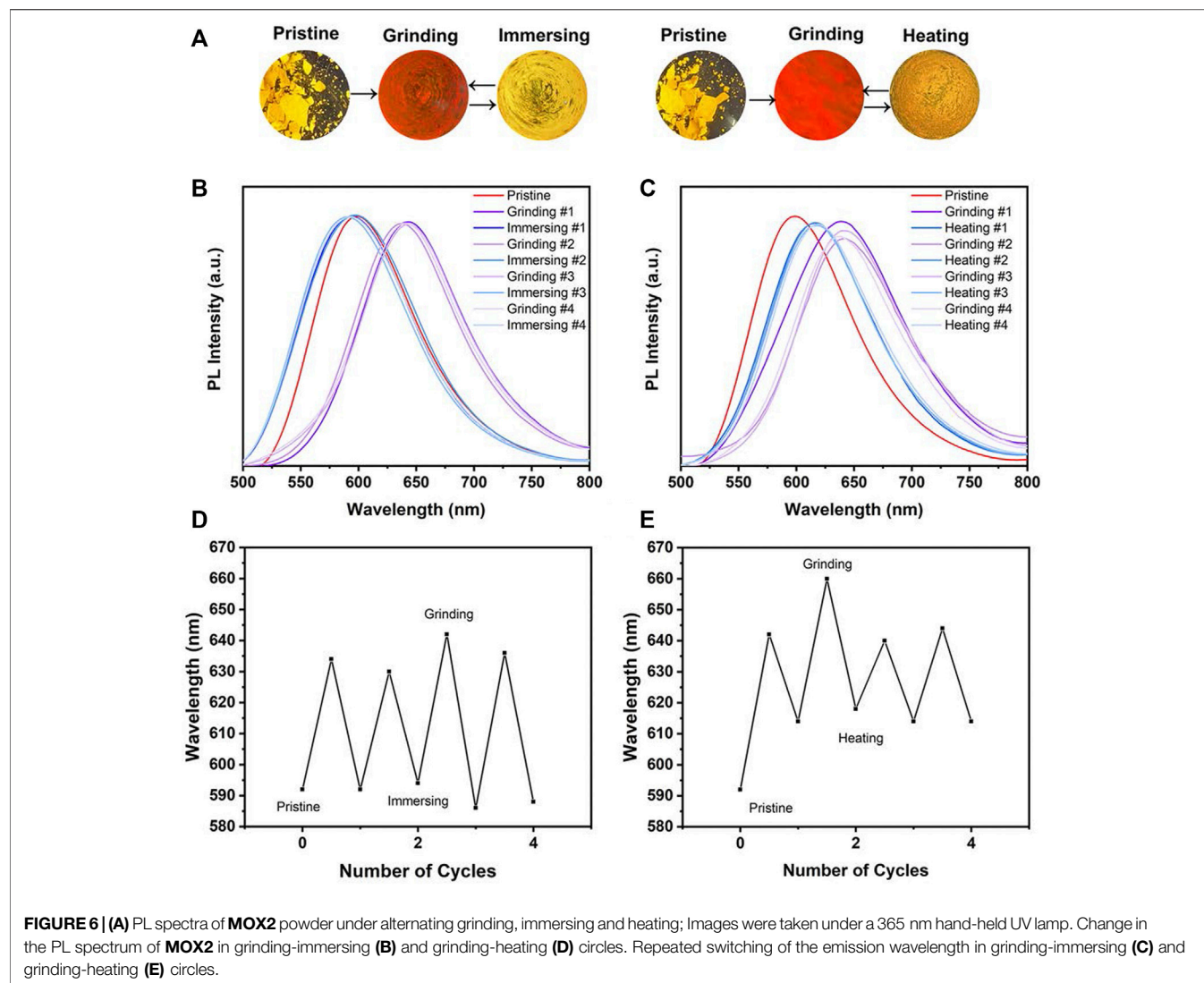


**TABLE 2 |** Peak emission wavelengths (nm) of solid-state **MOX2** under different conditions.

Compound	$\lambda_{pristine}$ (nm)	$\lambda_{grinding}$ (nm)	$\lambda_{immersing}$ (nm)	$\lambda_{heating}$ (nm)	$\Delta\lambda$ (nm)
<b>MOX2</b>	592	660	586	614	68

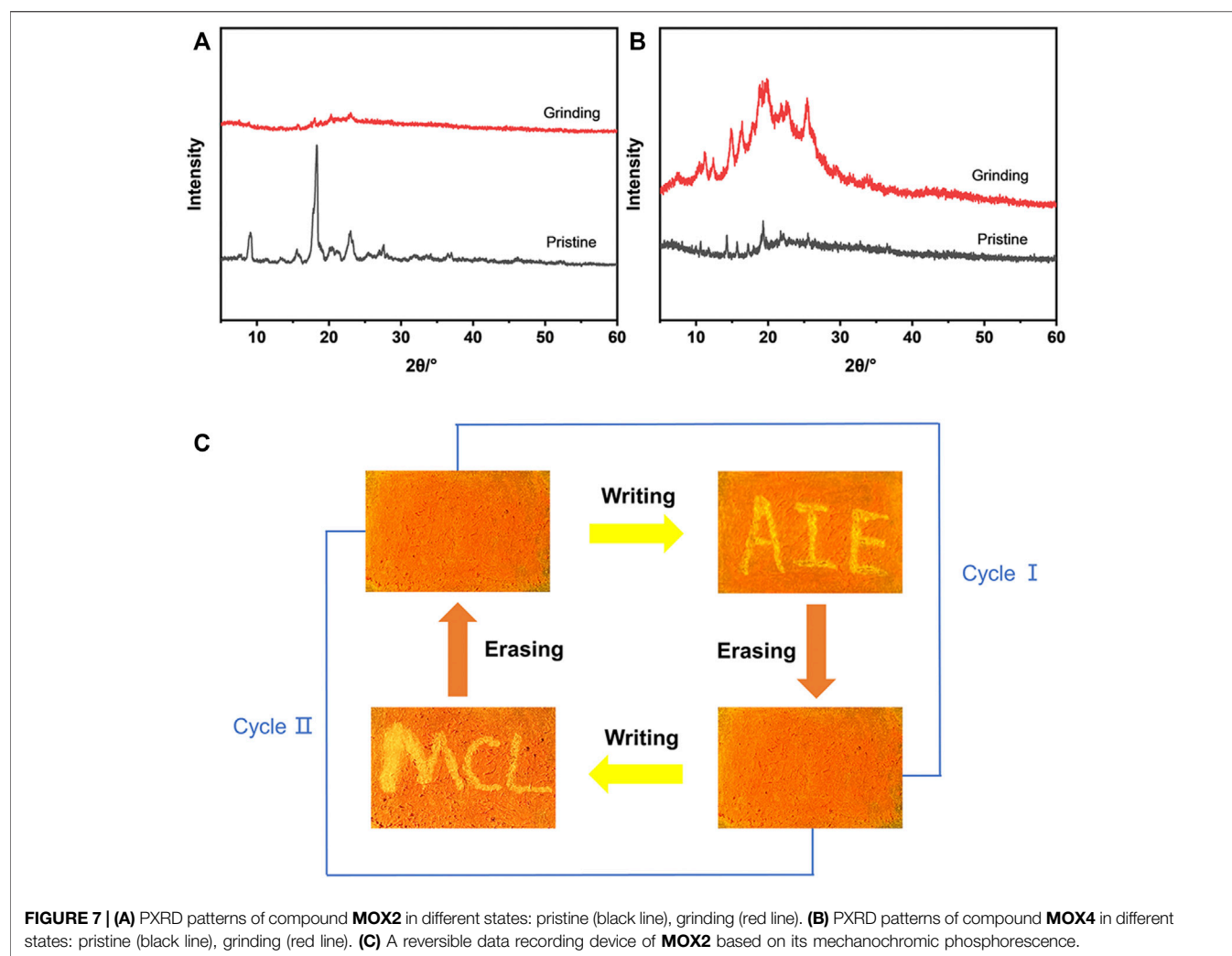
$$\Delta\lambda = \lambda_{pristine} - \lambda_{as-prepared}$$

changed from chloroform to DMSO, the  $\lambda_{em}$  of **MOX2**, and **MOX4** are red-shifted of 40 and 58 nm, respectively. Furthermore, the PL intensity of **MOX2** was gradually weakened with increased polarity of the solvent, indicating that the PL intensity of **MOX2** was highly dependent on the polarity of solvents.

### ACQ and AIE Properties of **MOX2** and **MOX4**

To demonstrate the feasibility of the present strategy, the photophysical properties of the two isomers were performed

to monitor the PL intensity fluctuation of the molecules in DMSO/water mixtures with various water volume fractions ( $f_w$ ) as shown in **Figure 4**. The absorption spectra as a function of the water fraction of **MOX2** and **MOX4** in DMSO as displayed in **Supplementary Figure S9**. As shown in **Figure 4C**, molecule **MOX4** displayed strong emission in DMSO due to the presence of a large  $\pi$ -conjugated planar structure. As  $f_w$  was increased from 0 to 100 vol%, the PL intensity was decreased gradually, and the quantum yield (QY) of **MOX4** decreased significantly from DMSO (3.96%) to water (0.30%) (**Table 1**). This result demonstrated that compound **MOX4** has typical ACQ effect. On the contrary, **MOX2** exhibited weak emission in DMSO (**Figure 4B**). In the water fraction range ( $f_w = 0-60$  vol%), the PL intensity was still weak. However, when  $f_w$  reached 80 vol%, the PL intensity was increased significantly, which was ascribed to the aggregation of the compound (**Figure 4D**) (Liu et al., 2016; Sun et al., 2018; Gao et al., 2019). Moreover, **MOX2** gave a low QY in pure DMSO (0.13%) but a high QY in pure water



(2.62%) (Table 1). Therefore, **MOX2** was AIE-active. The distinct difference in solid-state QY suggested a significant effect of the pyrrolidinyl position as regioisomers on the fluorescent properties.

### Crystal Analysis of **MOX2**

To better understand the origin of the AIE property, the single crystal of **MOX2** was obtained (CCDC 2107729) and its molecular packing was analyzed as follows. The crystal data and structure refinement for **MOX2** as displayed in Supplementary Table S2. As shown in Figure 5A, the dihedral angles between A-B, A-C, and B-C planes are 80.76°, 29.94°, and 65.82°, respectively. In addition, **MOX2** adopted a loose packing mode with weaker intermolecular C-H...O (2.484 Å, 2.696 Å, 2.633 Å, 2.659 Å) interactions as shown in Figure 5B; Supplementary Figure S10. The existence of these intermolecular interactions helped rigidify the molecular conformation, thus restricting the intramolecular rotation of the phenyl group. Moreover, the non-radiative relaxation process could be largely prohibited and significant emission enhancement was observed in its solid form, yielding the

remarkable AIE phenomenon. It is worth noting that such relatively weak intermolecular interactions could be easily destroyed upon exposure to external mechanical force, giving rise to the mechanochromic properties as studied below. The single crystal data of **MOX2** was displayed in the Supporting Information (Supplementary Table S2).

### Mechanochromic Properties of **MOX2**

Due to the AIE characteristics of **MOX2**, its mechanochromic luminescence (MCL) behaviors was investigated. As shown in Figure 6, the pristine **MOX2** powder emitted strong yellow fluorescence with a maximum at 592 nm. The emission peak red-shifted to 660 nm after grinding with red emission under 365 nm light. The spectral shift value was 68 nm (Table 2). The emission of the ground sample was restored to its original yellow color by immersing of acetone for 2 s or heated at 50°C within 10 min (Figure 6A). Moreover, fluorescence color conversion could be repeated numerous times (Figures 6B–E) without fatigue (Chan et al., 2014). To gain insight into the MCL phenomenon, PXRD and DSC experiments were conducted on the pristine, grinding, immersing, and heating solids of **MOX2**

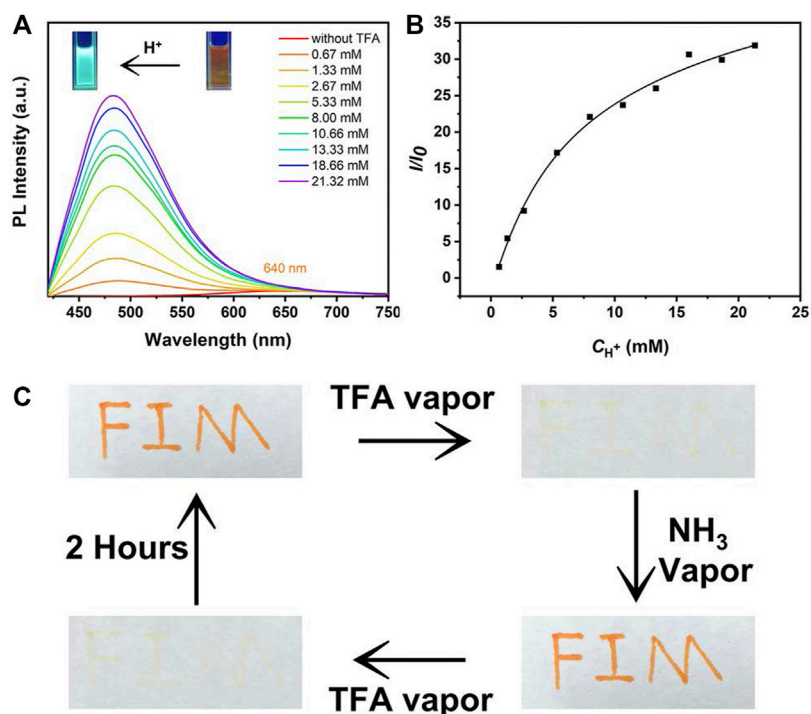


**FIGURE 8 | (A)** PL spectra of **MOX2** (100  $\mu\text{M}$ ) in methanol solvent with different concentration (0.67–21.32 mM) of TFA. Photographs of **MOX2** (100  $\mu\text{M}$ ) in methanol solvent before and after acidification at 365 nm UV light showed in the inset. **(B)** The plot and linear fitting of PL intensity at 484 nm versus TFA (0.67–21.32 mM). **(C)** Photographs of filter papers coated with **MOX2** (10 mM) in DCM solvent under different conditions.

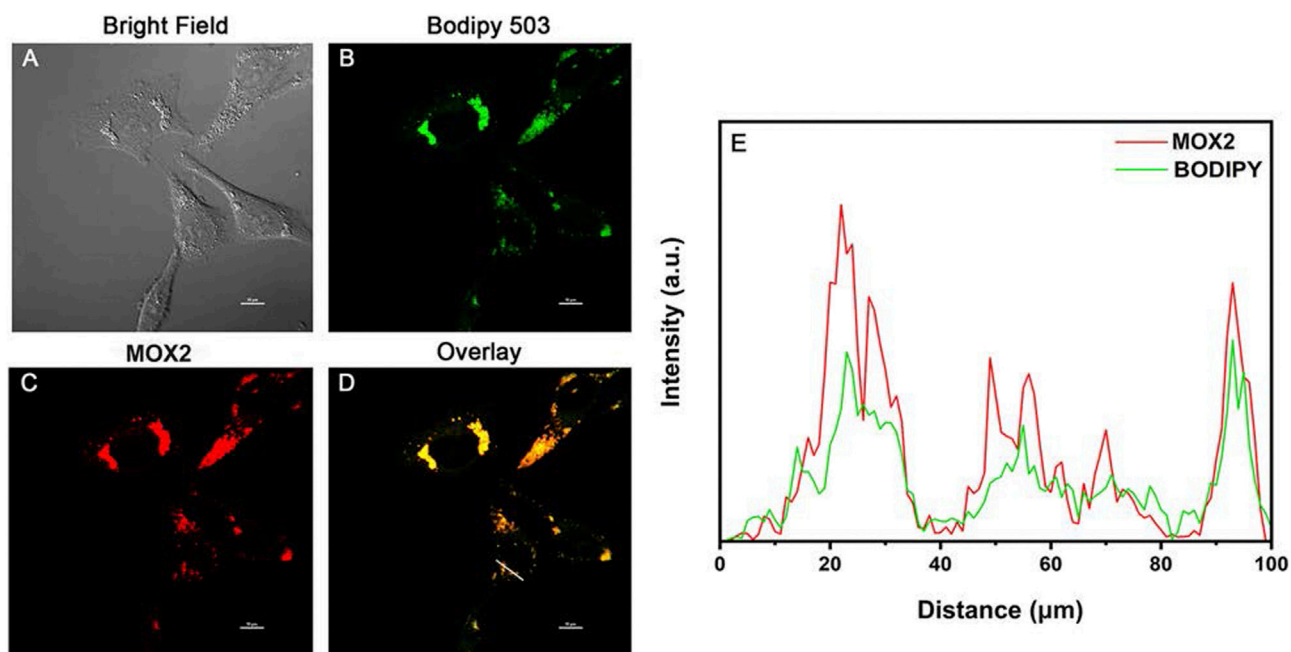
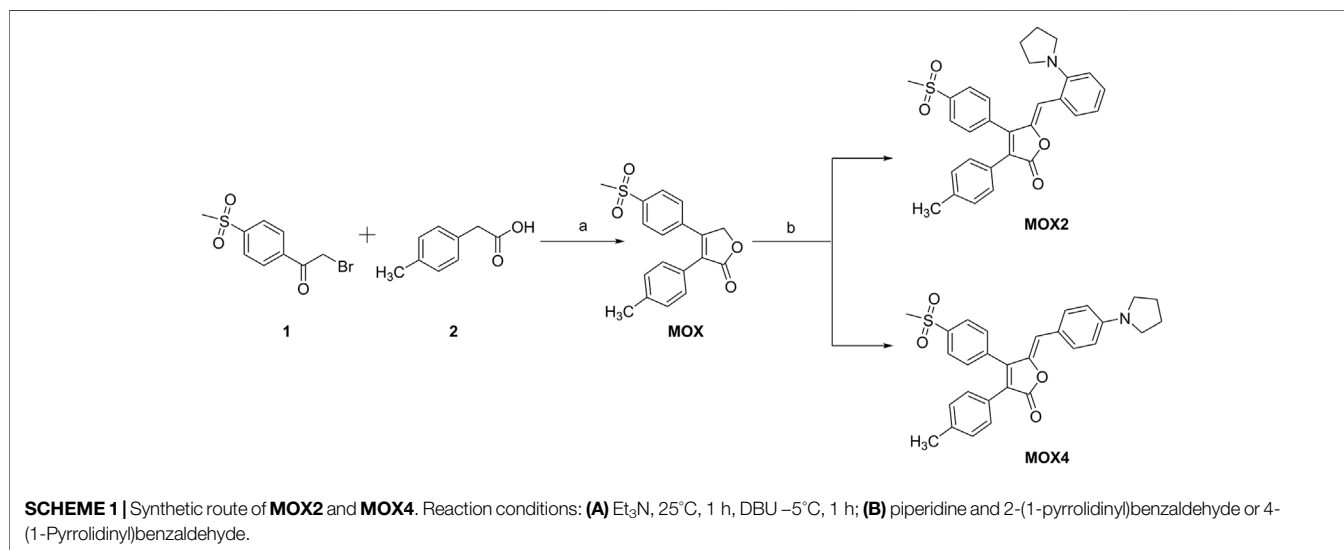


**FIGURE 9 |** Colocalization confocal imaging of living HeLa cells stained with **MOX2** and BODIPY 503: **(A)** bright field image; **(B)** imaging channel of BODIPY 503 ( $\lambda_{\text{ex}}$  = 488 nm;  $\lambda_{\text{em}}$  = 500–540 nm); **(C)** imaging channel of **MOX2** ( $\lambda_{\text{ex}}$  = 488 nm;  $\lambda_{\text{em}}$  = 600–640 nm); **(D)** overlay image. Scale bar: 10  $\mu\text{m}$ . **(E)** Red and green lines represent the fluorescence of **MOX2** and BODIPY, respectively.



and **MOX4** (Figure 7). It showed that the intensity of the diffraction peaks observed for powdered crystalline **MOX2** significantly decreased upon grinding, which indicated the loss of crystallinity. The diffraction peaks of **MOX4** still existed after heavily grinding. Furthermore, **MOX2** exhibited greater redshift than **MOX4** after grinding (Supplementary Figure S11). The transition from a crystalline structure to an amorphous state upon grinding was further confirmed by DSC experiments. In a DSC measurement of grinding **MOX2** and **MOX4** (Supplementary Figure S12), exothermic peaks that corresponded to the cold-crystallization transition **MOX2** ( $T = 107.7^{\circ}\text{C}$ ) and **MOX4** ( $T = 155.1^{\circ}\text{C}$ ) were observed followed by endothermic peaks that corresponded to the melting point of powder **MOX2** ( $T = 203.6^{\circ}\text{C}$ ) and **MOX4** ( $T = 231.3^{\circ}\text{C}$ ), respectively. These experimental results suggested that the transformation between crystalline structure and the amorphous state was responsible for the observed MCL behavior upon external stimuli.

By exploiting the excellent MCL behavior and good reversibility of **MOX2**, a simple rewritable phosphorescence data recording device was fabricated (Figure 7C) (Gundu et al., 2017). The specific reversible procedure is as follows. First, the original sample was put into a mortar and ground as the grinding sample. Next, it was spread on a filter paper to make a thin film, showing orange emission under UV excitation. Then, the characters “AIE” were written on the thin film with a writing brush with the acetone solvent as the “ink”. Due to the change of the emission color, the yellow-emitting letters could be clearly seen. Next, the “AIE” was erased by using a cotton swab to make it completely disappear, resulting in the recovery of the original orange thin film. New letters “MCL” could be written again with the “writing brush” of the acetone solvent, which could still be removed by using a cotton swab according to the above method. This writing-erasing process can be repeated for several cycles. Based on this, **MOX2** could be a potential fluorescent material for applications as repeated writing.

### Sensing Properties Toward Protonic Acids

Next, the sensing properties of **MOX2** was exploited because the pyrrolidine unit can be protonated. The solution of **MOX2** was prepared in DCM at a concentration of 1 mM. This solution was added dropwise to a filter paper. At this point, the filter paper showed a dark red color under 365 nm illumination. Then after fumigation with trifluoroacetic acid (TFA) for 1 min, at the very beginning, the filter paper exhibited light blue under 365 nm illumination. With the passage of time, the light blue faded, and then the orange began to appear (Supplementary Figure S13). Until 480 min, the blue was completely gone. The color of the filter paper sheet returned to orange (Supplementary Figure S13) (Chen et al., 2018). Meanwhile, as shown in Figure 8A, to investigate the possible acidochromic properties of **MOX2**, the spectral response ability of **MOX2** towards TFA in methanol solution ( $1.0 \times 10^{-4} \text{ M}$ ) was also measured. When TFA was gradually added to the methanol solution of **MOX2**, the yellow solution by degrees converted into a light blue one (Figure 8A inset). Upon addition of TFA, the color of **MOX2** in methanol solvent changed from orange to blue under 365 nm illumination, and a new blue-shifted peak formed in the PL spectrum (Figure 8A) (Cao et al., 2019; Cao et al., 2021). With the concentration of TFA increased from 0 to 21.32 mM, pronounced changes in emission suggested that **MOX2** had been protonated by TFA. The ratio of PL intensity had a quadratic relationship with TFA concentration in a certain range of TFA concentrations (Figure 8B) (Cao et al., 2020). As displayed in Figure 8C, we further explored the acidochromic behavior of **MOX2** for making a rewritable media by coating the solution on a filter paper. The letters were written on filter paper were stable, which could be erased only on fuming with TFA. Fumigation with ammonia could quickly return the sample to the initial color. Fumigation with TFA again can be quickly wiped off. The color would gradually return to its initial appearance after 2 h. This demonstrated that **MOX2** has the potential to be used as security link.

## Lipid Droplets Imaging in Living Cells

Lipid droplets (LDs) are key organelles which are closely related to living status and death process of living cells (Kuerschner et al., 2008; Walther and Farese, 2009). Before cell imaging experiments, the potential cytotoxicity of MOX2 and MOX4 was evaluated using the MTT assay and low cytotoxicity of them was observed (**Supplementary Figure S14**). We first conducted co-staining experiments of LDs in living HeLa cells (**Figure 9**). The cells were stained with BODIPY 503 ( $1 \times 10^{-5}$  M) and MOX2 ( $1 \times 10^{-5}$  M) for 0.5 h, and were imaged in green channel ( $\lambda_{ex} = 488$  nm,  $\lambda_{em} = 500$ –540 nm) and red channel ( $\lambda_{ex} = 488$  nm;  $\lambda_{em} = 600$ –640 nm), respectively. The two channels are well overlapped with each other. This result indicated the good LDs selectivity of MOX2. When HeLa cells were incubated with MOX2 for 30 min at 37°C, strong red fluorescence signals were observed from inside cells shown in **Supplementary Figure S15**. This was not surprising for the far-red emitting compound MOX2, which showed a bright fluorescence image *in vitro*.

## CONCLUSION

In this work, ACQ-to-AIE transformation was achieved by migrating a small pyrrolidinyl group from *para*- to *ortho*-position in a new molecular system, in which the *para*-isomer MOX4 showed the ACQ behavior and the *ortho*-isomer MOX2 is AIE-active. Moreover, compound MOX2 exhibited mechanochromic properties and pressure sensing ability. PXRD and DSC revealed that the MCL mechanism was ascribed to the transformation among crystalline state and the amorphous state by grinding. Furthermore, investigation of the acidochromic behavior of MOX2 revealed that it could be further used as security link. In further biological experimental study, MOX2 could be utilized as a fluorescent probe for LDs imaging in living cells. This work provides a novel strategy to achieve the ACQ-to-AIE transformation, which will provide a

## REFERENCES

- Arathi, A. S., Mallick, S., and Koner, A. L. (2016). Tuning Aggregation-Induced Emission of 2,3-Naphthalimide by Employing Cyclodextrin Nanocavities. *ChemistrySelect* 1, 3535–3540. doi:10.1002/slct.201600840
- Cao, Y., Xi, W., Wang, L., Wang, H., Kong, L., Zhou, H., et al. (2014). Reversible Piezofluorochromic Nature and Mechanism of Aggregation-Induced Emission-Active Compounds Based on Simple Modification. *RSC Adv.* 4 (47), 24649–24652. doi:10.1039/C4RA03042G
- Cao, X., Ding, Q., Li, Y., Gao, A., and Chang, X. (2019). Continuous Multi-Channel Sensing of Volatile Acid and Organic Amine Gases Using a Fluorescent Self-Assembly System. *J. Mater. Chem. C* 7, 133–142. doi:10.1039/c8tc04964e
- Cao, X., Li, Y., Han, Q., Gao, A., Wang, B., Chang, X., et al. (2020). Design of Large  $\pi$ -conjugated  $\alpha$ -cyanostilbene Derivatives as Colorimetric Sensors for Volatile Acids and Organic Amine Gases. *J. Mater. Chem. C* 8, 4058–4064. doi:10.1039/c9tc06148g
- Cao, X., Gao, A., Hou, J.-t., and Yi, T. (2021). Fluorescent Supramolecular Self-Assembly Gels and Their Application as Sensors: A Review. *Coord. Chem. Rev.* 434, 213792. doi:10.1016/j.ccr.2021.213792

new guideline for future design of new AIEgens from ACQ molecules.

## DATA AVAILABILITY STATEMENT

The original contributions presented in the study are included in the article/**Supplementary Material**, further inquiries can be directed to the corresponding authors.

## AUTHOR CONTRIBUTIONS

ZW, RL, LC performed the fluorescence and mass spectrometry experiments, and wrote the manuscript. XZ, WL, XL, and LWC performed data collation. NC, SS, ZL, and JH reviewed manuscript drafts. ZW, RL, and LC contributed equally in this work. XC, BL, and LX conceived the entire project.

## FUNDING

Financial support from the Natural Science Foundation of Fujian Province (No. 2020J06028) to LX and the NSFC (NO. 51872048) to RL, the CAS/SAFEA International Partnership Program for Creative Research Teams to XC and National Natural Science Foundation of China (Nos. 81872751 and 82104003). Liao Ning Revitalization Talents Program (No. XLYC2002115) and Key R&D Plan of Liaoning Province in 2020 (No. 2020020215-JH2/103).

## SUPPLEMENTARY MATERIAL

The Supplementary Material for this article can be found online at: <https://www.frontiersin.org/articles/10.3389/fchem.2021.823519/full#supplementary-material>

- Chan, C. Y. K., Lam, J. W. Y., Zhao, Z., Chen, S., Lu, P., Sung, H. H. Y., et al. (2014). Aggregation-Induced Emission, Mechanochromism and Blue Electroluminescence of Carbazole and Triphenylamine-Substituted Ethenes. *J. Mater. Chem. C* 2 (21), 4320–4327. doi:10.1039/C4TC00097H
- Chang, Z.-F., Jing, L.-M., Wei, C., Dong, Y.-P., Ye, Y.-C., Zhao, Y. S., et al. (2015). Hexaphenylbenzene-Based,  $\pi$ -Conjugated Snowflake-Shaped Luminophores: Tunable Aggregation-Induced Emission Effect and Piezofluorochromism. *Chem. Eur. J.* 21 (23), 8504–8510. doi:10.1002/chem.201406311
- Chen, L., Jiang, Y., Nie, H., Lu, P., Sung, H. H. Y., Williams, I. D., et al. (2014). Creation of Bifunctional Materials: Improve Electron-Transporting Ability of Light Emitters Based on AIE-Active 2,3,4,5-Tetraphenylsiloles. *Adv. Funct. Mater.* 24 (23), 3621–3630. doi:10.1002/adfm.201303867
- Chen, S., Liu, W., Ge, Z., Zhang, W., Wang, K.-P., and Hu, Z.-Q. (2018). Dimethylamine Substituted Bisbenzocoumarins: Solvatochromic, Mechanochromic and Acidochromic Properties. *CrystEngComm* 20 (36), 5432–5441. doi:10.1039/C8CE01034J
- Choi, S.-K., Rho, J., Yoon, S. E., Seok, J.-H., Kim, H., Min, J., et al. (2020). Full Color Tunable Aggregation-Induced Emission Luminogen for Bioimaging Based on an Indolizine Molecular Framework. *Bioconjug. Chem.* 31 (11), 2522–2532. doi:10.1021/acs.bioconjchem.0c00467

- Dhokale, B., Jadhav, T., Mobin, S. M., and Misra, R. (2015). *Meso* Alkynylated Tetraphenylethylene (TPE) and 2,3,3-Triphenylacrylonitrile (TPAN) Substituted BODIPYs. *J. Org. Chem.* 80 (16), 8018–8025. doi:10.1021/acs.joc.5b01117
- Feng HT, H.-T., Yuan, Y.-X., Xiong, J.-B., Zheng, Y.-S., and Tang, B. Z. (2018). Macrocycles and Cages Based on Tetraphenylethylene with Aggregation-Induced Emission Effect. *Chem. Soc. Rev.* 47 (19), 7452–7476. doi:10.1039/C8CS00444G
- Feng X, X., Qi, C., Feng, H.-T., Zhao, Z., Sung, H. H. Y., Williams, I. D., et al. (2018). Dual Fluorescence of Tetraphenylethylene-Substituted Pyrenes with Aggregation-Induced Emission Characteristics for White-Light Emission. *Chem. Sci.* 9 (25), 5679–5687. doi:10.1039/C8SC01709C
- Gao, C., Hossain, M. K., Wahab, M. A., Xiong, J., Qiu, B.-M., Luo, H., et al. (2019). Understanding the Details of Aggregation-Induced Emission (AIE) Effect in D- $\pi$ -A Type Imidazolium-Based Compounds through the Stepwise Change of Rotatable Moieties. *Dyes Pigm.* 160, 909–914. doi:10.1016/j.dyepig.2018.08.032
- Gomez-Duran, C. F. A., Hu, R., Feng, G., Li, T., Bu, F., Arseneault, M., et al. (2015). Effect of AIE Substituents on the Fluorescence of Tetraphenylethene-Containing BODIPY Derivatives. *ACS Appl. Mater. Inter.* 7 (28), 15168–15176. doi:10.1021/acsami.5b05033
- Gundu, S., Kim, M., Mergu, N., and Son, Y.-A. (2017). AIE-active and Reversible Mechanochromic Tetraphenylethene-Tetradiphenylacrylonitrile Hybrid Luminogens with Re-writable Optical Data Storage Application. *Dyes Pigm.* 146, 7–13. doi:10.1016/j.dyepig.2017.06.043
- Hong, Y., Lam, J. W. Y., and Tang, B. Z. (2009). Aggregation-Induced Emission: Phenomenon, Mechanism and Applications. *Chem. Commun.* 29, 4332–4353. doi:10.1039/b904665h
- Hong, Y., Lam, J. W. Y., and Tang, B. Z. (2011). Aggregation-Induced Emission. *Chem. Soc. Rev.* 40 (11), 5361–5388. doi:10.1039/c1cs15113d
- Huang, M., Lu, H., Wang, K., Liu, B., Wang, M., Qiao, X., et al. (2021). A Facile Design of Azaanthracene Derivatives: ACQ-AIE Conversion and Blue-Shifted Mechanofluorochromic Emission. *Dyes Pigm.* 186, 108992. doi:10.1016/j.dyepig.2020.108992
- Kuerschner, L., Moessinger, C., and Thiele, C. (2008). Imaging of Lipid Biosynthesis: How a Neutral Lipid Enters Lipid Droplets. *Traffic* 9 (3), 338–352. doi:10.1111/j.1600-0854.2007.00689.x
- La, D., Bhosale, S. V., Jones, L. A., and Bhosale, S. V. (2018). Tetraphenylethylene-Based AIE-Active Probes for Sensing Applications. *ACS Appl. Mater. Inter.* 10 (15), 12189–12216. doi:10.1021/acsami.7b12320
- Lee, C., Yang, W., and Parr, R. G. (1988). Development of the Colle-Salvetti Correlation-Energy Formula into a Functional of the Electron Density. *Phys. Rev. B* 37 (2), 785–789. doi:10.1103/PhysRevB.37.785
- Li A, A., Liu, Y., Han, L., Xu, S., Song, C., Geng, Y., et al. (2019). Pressure-Induced Remarkable Luminescence-Changing Behaviours of 9, 10-Distyrylanthracene and its Derivatives with Distinct Substituents. *Dyes Pigm.* 161, 182–187. doi:10.1016/j.dyepig.2018.09.041
- Li J, J., Wang, J., Li, H., Song, N., Wang, D., and Tang, B. Z. (2020). Supramolecular Materials Based on AIE Luminogens (AIEgens): Construction and Applications. *Chem. Soc. Rev.* 49, 1144–1172. doi:10.1039/c9cs00495e
- Li P, P., Zhang, D., Zhang, Y., Lu, W., Zhang, J., Wang, W., et al. (2019). Aggregation-Caused Quenching-type Naphthalimide Fluorophores Grafted and Ionized in a 3D Polymeric Hydrogel Network for Highly Fluorescent and Locally Tunable Emission. *ACS Macro Lett.* 8 (8), 937–942. doi:10.1021/acsmacrolett.9b00337
- Li Y, Y., Liu, S., Ni, H., Zhang, H., Zhang, H., Chuah, C., et al. (2020). ACQ-to-AIE Transformation: Tuning Molecular Packing by Regioisomerization for Two-Photon NIR Bioimaging. *Angew. Chem. Int. Ed.* 59 (31), 12822–12826. doi:10.1002/anie.202005785
- Lim, S., Tang, B. Z., and Hong, Y. (2016). “AIE Luminogens for Visualizing Cell Structures and Functions,” in *Aggregation-Induced Emission: Materials and Applications*. Editors M. Fujiki, B. Liu, and B. Z. Tang (Washington, DC: American Chemical Society), 1227, 199–216. doi:10.1021/bk-2016-1227.ch008
- Liu, X., Qiao, Q., Tian, W., Liu, W., Chen, J., Lang, M. J., et al. (2016). Aziridinyl Fluorophores Demonstrate Bright Fluorescence and Superior Photostability by Effectively Inhibiting Twisted Intramolecular Charge Transfer. *J. Am. Chem. Soc.* 138 (22), 6960–6963. doi:10.1021/jacs.6b03924
- Liu, J., Zhang, C., Dong, J., Zhu, J., Shen, C., Yang, G., et al. (2017). Endowing a Triarylboron Compound Showing ACQ with AIE Characteristics by Transforming its Emissive TICT State to Be Dark. *RSC Adv.* 7 (24), 14511–14515. doi:10.1039/C7RA00426E
- Long, X., Wu, J., Yang, S., Deng, Z., Zheng, Y., Zhang, W., et al. (2021). Discovery of and Insights into One-Photon and Two-Photon Excited ACQ-To-AIE Conversion via Positional Isomerization. *J. Mater. Chem. C* 9 (35), 11679–11689. doi:10.1039/D1TC01963E
- Lou, X. Y., and Yang, Y. W. (2020). Aggregation-induced Emission Systems Involving Supramolecular Assembly. *Aggregate* 1, 19–30. doi:10.1002/agt2.1
- Lu, H., Xu, B., Dong, Y., Chen, F., Li, Y., Li, Z., et al. (2010). Novel Fluorescent PH Sensors and a Biological Probe Based on Anthracene Derivatives with Aggregation-Induced Emission Characteristics. *Langmuir* 26 (9), 6838–6844. doi:10.1021/la904727t
- Lu, Q., Li, X., Li, J., Yang, Z., Xu, B., Chi, Z., et al. (2015). Influence of Cyano Groups on the Properties of Piezofluorochromic Aggregation-Induced Emission Enhancement Compounds Derived from Tetraphenylvinyl-Capped Ethane. *J. Mater. Chem. C* 3 (6), 1225–1234. doi:10.1039/C4TC02165G
- Lu, H., Wang, K., Liu, B., Wang, M., Huang, M., Zhang, Y., et al. (2019). Systematic Oligoaniline-Based Derivatives: ACQ-AIE Conversion with a Tunable Insertion Effect and Quantitative Fluorescence “Turn-On” Detection of BSA. *Mater. Chem. Front.* 3 (2), 331–338. doi:10.1039/C8QM00543E
- Luo, J., Xie, Z., Lam, J. W. Y., Cheng, L., Tang, B. Z., Chen, H., et al. (2001). Aggregation-Induced Emission of 1-Methyl-1,2,3,4,5-Pentaphenylsilole. *Chem. Commun.* 18, 1740–1741. doi:10.1039/b105159h
- Ma, X., Sun, R., Cheng, J., Liu, J., Gou, F., Xiang, H., et al. (2016). Fluorescence Aggregation-Caused Quenching versus Aggregation-Induced Emission: A Visual Teaching Technology for Undergraduate Chemistry Students. *J. Chem. Educ.* 93 (2), 345–350. doi:10.1021/acs.jchemed.5b00483
- Mallick, S., Arathi, A. S., and Koner, A. L. (2017). Customized Tuning of Aggregation-Induced Emission of a Naphthalimide Dye by Surfactants and Cyclodextrin. *J. Colloid Interf. Sci.* 499, 46–53. doi:10.1016/j.jcis.2017.03.097
- Mei, J., Leung, N. L. C., Kwok, R. T. K., Lam, J. W. Y., and Tang, B. Z. (2015). Aggregation-Induced Emission: Together We Shine, United We Soar!. *Chem. Rev.* 115 (21), 11718–11940. doi:10.1021/acs.chemrev.5b00263
- Niu, C., You, Y., Zhao, L., He, D., Na, N., and Ouyang, J. (2015). Solvatochromism, Reversible Chromism and Self-Assembly Effects of Heteroatom-Assisted Aggregation-Induced Enhanced Emission (AIEE) Compounds. *Chem. Eur. J.* 21 (40), 13983–13990. doi:10.1002/chem.201501902
- Pati, A. K., Mohapatra, M., Ghosh, P., Gharpure, S. J., and Mishra, A. K. (2013). Deciphering the Photophysical Role of Conjugated Diyne in Butadiynyl Fluorophores: Synthesis, Photophysical and Theoretical Study. *J. Phys. Chem. A* 117 (30), 6548–6560. doi:10.1021/jp404809g
- Pati, A. K., Gharpure, S. J., and Mishra, A. K. (2015). On the Photophysics of Butadiyne Bridged Pyrene-Phenyl Molecular Conjugates: Multiple Emissive Pathways through Locally Excited, Intramolecular Charge Transfer and Excimer States. *Faraday Discuss.* 177, 213–235. doi:10.1039/C4FD00170B
- Pratihari, S., Bhattacharyya, A., and Prasad, E. (2020). Achieving ACQ-AIE Modulation Using Isostructural Organic Fluorophores. *J. Photochem. Photobiol. A Chem.* 396, 112458. doi:10.1016/j.jphotochem.2020.112458
- Ravindran, E., and Somanathan, N. (2017). Efficient white-light Emission from a Single Polymer System with “spring-like” Self-Assemblies Induced Emission Enhancement and Intramolecular Charge Transfer Characteristics. *J. Mater. Chem. C* 5 (19), 4763–4774. doi:10.1039/C7TC01036B
- Sasaki, S., Suzuki, S., Igawa, K., Morokuma, K., and Konishi, G.-i. (2017). The K-Region in Pyrenes as a Key Position to Activate Aggregation-Induced Emission: Effects of Introducing Highly Twisted N,N-Dimethylamines. *J. Org. Chem.* 82 (13), 6865–6873. doi:10.1021/acs.joc.7b00996
- Shen, X. Y., Wang, Y. J., Zhao, E., Yuan, W. Z., Liu, Y., Lu, P., et al. (2013). Effects of Substitution with Donor-Acceptor Groups on the Properties of Tetraphenylethene Trimer: Aggregation-Induced Emission, Solvatochromism, and Mechanochromism. *J. Phys. Chem. C* 117 (14), 7334–7347. doi:10.1021/jp311360p
- Sun, H., Tang, X.-X., Miao, B.-X., Yang, Y., and Ni, Z. (2018). A New AIE and TICT-Active Tetraphenylethene-Based Thiazole Compound: Synthesis, Structure, Photophysical Properties and Application for Water Detection in Organic Solvents. *Sensors Actuators B Chem.* 267, 448–456. doi:10.1016/j.snb.2018.04.022

- Walther, T. C., and Farese, R. V. (2009). The Life of Lipid Droplets. *Biochim. Biophys. Acta Mol. Cell Biol. Lipids* 1791 (6), 459–466. doi:10.1016/j.bbalip.2008.10.009
- Wang, Z., Wang, C., Fang, Y., Yuan, H., Quan, Y., and Cheng, Y. (2018). Color-Tunable AIE-Active Conjugated Polymer Nanoparticles as Drug Carriers for Self-Indicating Cancer Therapy via Intramolecular FRET Mechanism. *Polym. Chem.* 9 (23), 3205–3214. doi:10.1039/C8PY00329G
- Wang, H., Xing, H., Gong, J., Zhang, H., Zhang, J., Wei, P., et al. (2020). "Living" Luminogens: Light Driven ACQ-To-AIE Transformation Accompanied with Solid-State Actuation. *Mater. Horiz.* 7 (6), 1566–1572. doi:10.1039/D0MH00447B
- Wu, B., Xue, T., Wang, W., Li, S., Shen, J., and He, Y. (2018). Visible Light Triggered Aggregation-Induced Emission Switching with a Donor-Acceptor Stehouse Adduct. *J. Mater. Chem. C* 6 (31), 8538–8545. doi:10.1039/C8TC02621A
- Xiong, Y., Yan, X., Ma, Y., Li, Y., Yin, G., and Chen, L. (2015). Regulating the Piezofluorochromism of 9,10-Bis(Butoxystyryl)Anthracenes by Isomerization of Butyl Groups. *Chem. Commun.* 51 (16), 3403–3406. doi:10.1039/C4CC10196K
- Yuan, W. Z., Lu, P., Chen, S., Lam, J. W. Y., Wang, Z., Liu, Y., et al. (2010). Changing the Behavior of Chromophores from Aggregation-Caused Quenching to Aggregation-Induced Emission: Development of Highly Efficient Light Emitters in the Solid State. *Adv. Mater.* 22 (19), 2159–2163. doi:10.1002/adma.200904056
- Yuan, M.-S., Wang, D.-E., Xue, P., Wang, W., Wang, J.-C., Tu, Q., et al. (2014). Fluorenone Organic Crystals: Two-Color Luminescence Switching and Reversible Phase Transformations between  $\pi$ - $\pi$  Stacking-Directed Packing and Hydrogen Bond-Directed Packing. *Chem. Mater.* 26 (7), 2467–2477. doi:10.1021/cm500441r
- Zhang, X., Chi, Z., Zhang, J., Li, H., Xu, B., Li, X., et al. (2011). Piezofluorochromic Properties and Mechanism of an Aggregation-Induced Emission Enhancement Compound Containing N-Hexyl-Phenothiazine and Anthracene Moieties. *J. Phys. Chem. B* 115 (23), 7606–7611. doi:10.1021/jp202112e
- Zhang, Y., Sun, J., Lv, X., Ouyang, M., Cao, F., Pan, G., et al. (2013). Heating and Mechanical Force-Induced "turn on" Fluorescence of Cyanostilbene Derivative with H-type Stacking. *CrystEngComm* 15 (44), 8998–9002. doi:10.1039/c3ce41221k
- Zhang, H., Zhang, H., Huang, G., and Li, B. S. (2021). Two Tetraphenylethene-Pyrene Isomers: Distinct Fluorescence and Mechanochromic Properties. *Dyes Pigm.* 185, 108947. doi:10.1016/j.dyepig.2020.108947
- Zhang, X., Ma, Z., Yang, Y., Zhang, X., Jia, X., and Wei, Y. (2014). Fine-tuning the Mechanofluorochromic Properties of Benzothiadiazole-Cored Cyano-Substituted Diphenylethene Derivatives through D-A Effect. *J. Mater. Chem. C* 2 (42), 8932–8938. doi:10.1039/C4TC01457J
- Zhang, Y., Sun, J., Zhuang, G., Ouyang, M., Yu, Z., Cao, F., et al. (2014). Heating and Mechanical Force-Induced Luminescence On-Off Switching of Arylamine Derivatives with Highly Distorted Structures. *J. Mater. Chem. C* 2 (1), 195–200. doi:10.1039/C3TC31416B
- Zong, L., Xie, Y., Wang, C., Li, J.-R., Li, Q., and Li, Z. (2016). From ACQ to AIE: the Suppression of the strong  $\pi$ - $\pi$  Interaction of Naphthalene Diimide Derivatives through the Adjustment of Their Flexible Chains. *Chem. Commun.* 52 (77), 11496–11499. doi:10.1039/C6CC06176A

**Conflict of Interest:** The authors declare that the research was conducted in the absence of any commercial or financial relationships that could be construed as a potential conflict of interest.

**Publisher's Note:** All claims expressed in this article are solely those of the authors and do not necessarily represent those of their affiliated organizations, or those of the publisher, the editors and the reviewers. Any product that may be evaluated in this article, or claim that may be made by its manufacturer, is not guaranteed or endorsed by the publisher.

Copyright © 2022 Wang, Li, Chen, Zhai, Liu, Lin, Chen, Chen, Sun, Li, Hao, Chen, Lin and Xie. This is an open-access article distributed under the terms of the Creative Commons Attribution License (CC BY). The use, distribution or reproduction in other forums is permitted, provided the original author(s) and the copyright owner(s) are credited and that the original publication in this journal is cited, in accordance with accepted academic practice. No use, distribution or reproduction is permitted which does not comply with these terms.